A finite element analysis of tibial tritanium cones without stems in varying bone defects

A finite element analysis of tibial tritanium cones without stems in varying bone defects

Shuqiao Xie[1], Noel Conlisk[1], David Hamilton[2], Chloe Scott[3], Richard Burnett[3] and Pankaj Pankaj[1*]

[1]School of Engineering, Institute for Bioengineering, The University of Edinburgh, Alrick Building, The King's Buildings, Edinburgh EH9 3BF, UK

[2]Department of Orthopaedics and Trauma, The University of Edinburgh, 49 Little France Crescent, Edinburgh, EH16 4SB, UK

[3]Department of Orthopaedics and Trauma, Royal Infirmary of Edinburgh, 51 Little France Crescent, Edinburgh, EH16 4SB, UK

Corresponding author:

Professor Pankaj Pankaj

pankaj@ed.ac.uk

+44 (0) 131 650 5800

Abstract

Background: In the UK around 10% of hip and knee arthroplasties are revision operations. At revision total knee arthroplasty (rTKA), bone loss management is critical to achieving a stable bone-implant construct. Though tritanium cones have been used to manage bone defects in rTKA, their biomechanical performance with varying defects remains unknown.

Methods: Uncontained tibial bone defects at four anatomic locations, with varying depths and widths (Type T2A and T2B) were investigated computationally in a composite tibia which was subjected to four loading scenarios. The ability of the tritanium cone to replace the tibial bone defect was examined using the outcome measures of bone strain distribution and interface micromotions.

Results: It was found that anterior and lateral defects do not significantly alter the strain distribution compared with intact bone. For medial defects, strain distribution is sensitive to defect width; while strain distributions for posterior defects are associated with defect width and depth. In general, micromotions at the bone-implant interface are small and are primarily influenced by defect depth.

Conclusions: Our models show that the cone is an acceptable choice for bone defect management in rTKA. Since all observed micromotions were small, successful osteointegration would be expected in all types of uncontained defects considered in this study. Tritanium cones safely accommodate uncontained tibial defects up to 10mm deep and extending up to 9mm from the centre of the cone. Medial and posteriorly based defects managed with symmetric cones display the greatest bone strains and asymmetric cones may be useful in this context.

Keywords:

Bone defects; finite element analysis; micromotion; principal strain; revision knee arthroplasty

Introduction

Approximately one hundred thousand (100,000) knee arthroplasties are carried out in the UK each year, of which around 10% are revision operations [1,2]. Revision total knee arthroplasty (rTKA) surgery presents numerous challenges, of which bone defect management is a critical step in the achievement of a stable bone-implant construct and a successful clinical outcome [3,4].

Bone loss can be the result of: (1) aseptic failure with component loosening, subsidence, osteolysis, and fracture; (2) septic failure with bone resorption and osteolysis; or (3) iatrogenic bone loss following component removal [5]. There is still no agreement regarding the optimal management of bone loss. Bone grafts, tantalum augments, porous metaphyseal sleeves, and tantalum cones have all been advocated [6]. Structural bone grafts are a cost effective method of managing bone defects, and they also have the potential for bone stock restoration and ligamentous reattachment [6], though a high risk of infection has been reported [7,8]. Tantalum augments are quick and easy to use, allow immediate mobilisation and loading, and clinically display aseptic loosening rates of 7.6% at 7-years follow up [9]. Metaphyseal sleeves or tantalum cones provide a stable scaffold for joint reconstruction for large bone defects, decrease the complexity of the reconstruction, and enable immediate mobilisation [10]. Multiple studies have demonstrated favourable short-term outcomes using tantalum cones in clinical [11] and experimental [12] settings, but these require the removal of a considerable amount of host bone for implant positioning.

Tritanium metaphyseal cones have been designed to replace lost bone in rTKA. They have been shown to have comparable or superior fixation compared to tantalum cone systems in an experimental study, which measured micromotions under physiological loading [13]. A recent clinical study of 62 rTKAs confirmed the newly developed cones to be effective at restoring joint stability with no cases of aseptic loosening at a mean of 27-months follow up [14]. To the authors' knowledge, the biomechanical performance of tritanium cones in tibiae with different locations and severity of bony defects has not previously been investigated.

The main aim of this study is to examine, through numerical simulation, the performance of tritanium cones in the presence of commonly observed tibial defects using bone strain and bone-implant interface micromotion as outcome variables. Uncontained defects at different anatomic locations and with different size/width and/or depth (Anderson Orthopaedic Research Institute (AORI) classification T2A and T2B) are considered.

Materials and Methods

Geometry

A three-dimensional computer-aided design (CAD) model of the tibia was obtained from a previous study [15]. A generic bone geometry was employed in this study. A patient specific model was not selected so as to emphasise the biomechanical performance of the implant in the presence of different bone defects rather than the influence of an individual's bone geometry and properties. To accommodate rTKA, the bone in the tibial model was resected at a depth of 8mm below the medial articular surface (to account for the primary TKA resection and subsequent removal of the tibial baseplate) and was aligned perpendicular to the mechanical axis of the tibia (consistent with intramedullary alignment), with 0 degrees of posterior tibial slope and rotation coincident with a line from the PCL recess to the tibial tuberosity. Universal Tibial Baseplate #3 (5521-B-300) was chosen in this study and Triathlon Tritanium Symmetric Cone Augment (Stryker Orthopaedics, Marwah, NJ, USA) Size A (5549-A-110) was considered as per the recommended surgical technique. The dimensions of the baseplate and cone used in the current study can be found in the manufacturer's specifications. To avoid any direct contact between the baseplate and the cone, a 2mm thick cement layer was included and cement was filled up from the bottom of the cone (Fig. 1a).

A series of uncontained bone defects were considered in this study, consistent with Anderson Orthopaedic Research Institute (AORI) classification T2A and T2B defects. Defects at four anatomical locations were included: anterior, lateral, medial and posterior, denoted as A, L, M and P respectively. Defect width was defined as the distance from the centre of the cone to the edge where the bone defect appears (Fig 1b). The cone selected had a distal diameter of 18mm and a proximal outer diameter of 33mm (Fig 1a). Bone defects with three widths from 9mm to 15mm at 3mm increments were considered (Fig. 1b). It is important to note that for defects of different widths the smaller value in defect notation represents a larger defect or bone loss (i.e. defect M9 has more bone loss than M12). Defect depth is simply defined as the depth of the defect measured from the sectioning plane (proximal plateau resection) along the inferior direction (Fig. 1c), two bone defect depths were considered – 5mm and 10mm. A notation that included both width and depth of defect was adopted. For example, M9D5 means that defect exists in the medial direction and starts 9mm away from the centre of the cone and has a depth of 5mm Twenty-five models were created; 24 models with different defects and 1 control model which had no defects (denoted as NO).

The geometry was meshed with linear tetrahedral elements with an average element edge length of 1 mm (total number of elements range: 668,507 – 943,320 elements) with refinement at the bone-implant interface (with an edge length of ~0.5 mm). Mesh convergence studies demonstrated that further mesh refinement increased both maximum displacement and bone strain by less than 0.5 %.

Material definitions

The materials were assumed to be homogeneous, isotropic and linear elastic (Table 1). Poisson's ratio of 0.3 was assumed for all materials.

Fully-bonded interfaces were assumed where any region of the bone-implant construct contacted with cement (i.e. baseplate to cement, cement to cone and cement to bone); surface-to-surface frictional contact was assumed at bone-implant interfaces. A standard Coulomb friction coefficient of 0.35 [16–19] was employed for contacts between baseplate and tritanium cone to bone, while coefficient of 1.01 [20] was assumed for the contact between tritanium cone coating and bone.

Table 1 Material properties used

Parts	Young's modulus E(MPa)	Poisson's ratio ν
Cortical bone [21]	15,250	0.3
Trabecular bone	449	
Tibial baseplate	210,000	
Bone cement [22]	2,280	
Titanium cone [23]	117,000	
Tritanium cone coating [23]	6,200	

Loading and boundary conditions

The force components $+F_x$, $+F_y$ and $+F_z$ act in lateral, anterior and inferior directions and positive moment components were defined accordingly, as shown in Fig. 1c. The forces and moments were applied to a reference point which was at the centre of the tibial baseplate and was constrained with the top surface of the baseplate using multi-point constraints. Standard average loads for the knee joint in subjects with 75 kg body weight were chosen from OrthoLoad [24]. Four loading scenarios were selected for the current study: knee bend (squatting), standing up, walking and stair descent (denoted as KB, SU, WA and StaD respectively), activities which cover a majority of the loading conditions encountered during a patient's activities of daily living. The time-points with the largest superior-inferior forces (F_z) were chosen for WA and KB and the time-points having the largest M_x

for StaD and KB were considered. Forces and moments for all loading scenarios considered in this study are illustrated in Fig. 2. Similar to many previous studies [25,26], the tibia was truncated and fixed in all degrees of freedom at a distance of 200mm (measured from the sectioning plane, as shown in Fig. 1c.

The biomechanical performance of the rTKA implant construct was assessed using bone strain and micromotion at the bone-implant interface as outcome measures. Micromotion relates to the immediate stability of the implant system and is also an indicator of long-term stability. To evaluate micromotions, corresponding nodes between implants (tibial baseplate and two parts of the cone) and neighbouring bone were paired to produce the implant-bone node-pairs by using a customised MATLAB code (MathWorks, US). The micromotions were defined as displacements at these node-pairs due to load application.

Results

Twenty-four different bone defects (bone loss scenarios) were considered in this study. Of the defects modelled in this study, the most severe posterior bone defect (P9D10) involved the largest volume of bone loss (Fig. 3). Bone defects involved the loss of 0.44% (defect A15D5) to 6.36% (defect P9D10) of the total volume of the intact bone. Lateral and medial defects resulted in similar volumes of bone loss for defects with the same width and depth (e.g. L9D5 and M9D5).

Principal strain rather than stress was used for the comparison [27–29] and the strain limits of >0.2% (tensile) and <-0.2% (compressive) for maximum and minimum principal strains, respectively [30] were employed. These values are close to the upper limit of physiological strain [30]. In general, there were two regions of the bone, which experienced high strain: (a) the posterior region of the tibial shaft and (b) the proximal tibia as shown in Fig. 4. Contour maps of the superior cut tibial surface demonstrating maximum (Fig. 4a) and minimum (Fig. 4b) principal strains are given in Figure 4 for bone defects in each direction. The ratio ($\%V_\epsilon$) of the volume of bone that exceeded the preselected principal strain magnitude ($V_{\varepsilon_{min}<-0.2\%} \cup V_{\varepsilon_{max}>0.2\%}$) to the total volume of bone with defect (Eq. 1) are shown in Fig. 5 for each of the loading scenarios for all bone defects considered (Fig. 5).

$$\%V_\epsilon = \frac{V_{\varepsilon_{min}<-0.2\%} \cup V_{\varepsilon_{max}>0.2\%}}{V_{bone\ wih\ defect}} \times 100 \quad (1)$$

Similar $\%V_\epsilon$ were found for all types of bone defects. In general, for different loading scenarios significant differences in $\%V_\epsilon$ were observed. From KB (Fig. 5a), SU (Fig. 5b), WA (Fig. 5c) to StaD (Fig. 5d) the volume increased, with the highest occurring for StaD.

The typical micromotion patterns for bone with no defect and for the most severe defect from each anatomic direction are shown in Fig. 6 for each of the four loading scenarios. It was found that relatively higher micromotions occur at the location closest to the defect and in the posterior region of the bone. The highest micromotion of 37.1 μm was found for bone with an M9D10 defect when subjected to WA loading (Fig. 6). Micromotions at the bone-implant interface were grouped in ranges: < 15 μm, 15-25 μm and 25-40 μm. The percentage of surface areas which lie in these ranges to total areas of the bone-implant interface were calculated and are shown in Fig. 7. Micromotions less than 15 μm were excluded.

Anterior defects

The strain distribution for bone with the most severe anterior defect was similar to bone with no defect (Fig. 4). The volume of bone loss was 0.44% and 2.13% for A15D5 and A9D10 respectively, but the change in the size and depth of these defects did not significantly alter strain distribution for any of the loading scenarios considered (Fig. 5).

The anterior and posterior regions of bone experienced relatively larger micromotions compared to the bone with no defect (Fig. 6). More than 90% of the bone-implant surfaces experienced micromotion less than 15 μm. The highest micromotions for this defect were observed when the bone-implant construct was subjected to WA load (Fig. 7).

Lateral defects

Larger minimum principal (compressive) strains were observed in the trabecular bone where contact occurred with the bottom of the cone when the bone-implant construct was subjected to KB and SU loadings (Fig. 4b). No significant difference in strain distribution or maximum principal strain was observed when WA or StaD loadings were applied (Fig. 4). Slightly larger $\%V_\epsilon$ were found for KB (Fig. 5a) and SU (Fig. 5b) compared to the bone without defect, though the highest was below 6%. A similar $\%V_\epsilon$ was found for bone with/without defect under WA and StaD loadings.

For bone with lateral defects, relatively higher micromotions were found with SU loading but the magnitude remained small (Fig. 6). More than 80% of the area had micromotions less than 15 μm. SU resulted in the

highest micromotions for this defect type, and it was sensitive to the depth of defect (Fig. 7b). Almost no difference in micromotion was found when comparing WA (Fig. 7c) and StaD (Fig. 7d) loadings with the bone with no defect.

Medial defects

For KB and SU loadings, considerable differences in strain distribution were observed compared to bone with no defect (Fig. 4). WA and StaD resulted in more bone exceeding the preselected strain range. Interestingly, this $\%V_\epsilon$ was found to be more sensitive to defect width rather than depth (Fig. 5c and 5d). The largest differences in strain distribution were found for StaD loading (Fig 4) with a significantly larger value of $\%V_\epsilon$ for this loading scenario (Fig. 5d). Considering defects of the same width and depth, medial bone defects resulted in a much higher value of $\%V_\epsilon$ for WA and StaD compared to lateral defect (i.e. M9D5 has a higher volume of bone exceeding the range than L9D5 for WA and StaD loadings).

WA and StaD loading scenarios resulted in the largest micromotions at the bone-implant interface, with larger micromotions found close to the location of the defect (Fig. 6). Though more than 95% of surfaces had micromotions less than 15 μm for KB (Fig. 7a) and SU (Fig. 7b) loadings, larger areas of the bone-implant interface experienced medium range micromotions (15-25 μm) at the WA loading and high range micromotions (25-40 μm) at StaD loading. Again, this micromotion was found to be more sensitive to the depth of the defect rather than the width.

Posterior defects

Comparing strain patterns from the most severe posterior defect of the bone with the no defect scenario, higher strains were observed for bone with posterior defects, especially for WA and StaD loading cases. The strain was concentrated in the posterior region (i.e. location of the defect) (Fig. 4). Considerable increase in $\%V_\epsilon$ was found for all loading scenarios (Fig. 5) and was associated with both defect depth and width, i.e. for each loading scenario, P9D10 has considerably higher value of $\%V_\epsilon$ than P9D5, while P12D5 has a smaller value of $\%V_\epsilon$ than P9D5.

Relatively higher micromotions were found close to the defect location for all loading scenarios (Fig. 6). The majority (more than 95%) of surfaces had micromotions less than 15 μm when subjected to KB and SU loadings (Fig. 7). WA and StaD loading resulted in relatively higher micromotions at the interface, however, overall these motions remain small with almost no high range micromotions (25-40 μm) observed. It is noted that

196 although posterior defects give the largest percentage of bone loss, the observed micromotion is generally
197 smaller than medial defects of the same width and depth. Micromotions at the interface were associated with
198 both depth and width.

199 ## Discussion

200 The models in the current study show that tritanium cones are an acceptable choice for bone loss management in
201 rTKA surgery. By examining strain distribution and micromotions at the bone-implant interface, it is clear that
202 these devices perform well by not only filling large bone voids but also by restoring comparable implant
203 performance in comparison to bone without defects. Strain distribution in cortical bone is similar for each
204 loading scenarios and there are only small differences for different defect variations (i.e. width, depth). Anterior
205 defects have almost no effect on stability of the bone-implant system based on examining the principal strains
206 and the observed micromotions at interface. The values of $\%V_\epsilon$ were small for KB and SU. For WA and StaD
207 loadings, there was no significant difference in the volume exceeding the preselected strain range for anterior
208 and lateral defects compared to the no defect scenario. Despite approximately similar volumes of bone being
209 removed at each defect location except at the anterior, significant increases in $\%V_\epsilon$ were observed only for
210 medial and posterior defects, and especially for WA and StaD loadings. The volume of bone exceeding the
211 preselected strain range was found to be sensitive to defect width for medial defects and both width and depth
212 for posterior defects. Overall, micromotions at the bone-implant interface were small (highest ~37 μm) for all
213 models considered in this study. The higher micromotions from each of the loading scenarios are more likely to
214 be influenced by the depth of defects.

215 **Table 2 Summary of how defect affects strain distribution of bone**

Loading scenario	Defect			
	Anterior [1]	Lateral [2]	Medial	Posterior
Knee Bend (KB)	-	Width	-	-
Standing Up (SU)	-	Width	-	-
Walking (WA)	-	-	Width	Width + Depth
Descending Stairs (StaD)	-	-	Width	Width + Depth

[1] anterior defect has a limited effect on the volume of bone greater than preselected strain range compared to no defect case

[2] volumes of bone greater than preselected strain range were small but trends are apparent

- almost no difference compared to the bone without defect - will not be discussed

216

Theoretically, for a given constant force applied to a surface, the experienced strain will increase as the area of the load application surface is decreased. Considering the combinations of forces and moments applied to bone-implant constructs (Fig. 2), larger forces were applied in the posterior direction (i.e. $-F_y$) for WA and StaD loading scenarios. With increased defect depth, the contact area between the implant and the bone is decreased significantly. This is also the case as defect width is increased. This explains that bone's strain distribution is associated with defect depth and width for bone with posterior defects.

Similarly, the lever arm is an important parameter for a system subjected to bending moments. For a constant bending moment applied, larger strains will occur in a system with a smaller lever arm. In our bone-implant construct, the level arm is represented by defect width. Smaller defect width resulted in a larger lever arm, e.g. M15D5 has a larger lever arm than M9D5. WA and StaD loading scenarios have large positive moments M_y: the strain distribution for bone with a medial defect is therefore associated with defect width rather than depth. On the other hand, for a posterior defect, the variation of defect width also contributes to the variation in strain distribution as there were large moments M_x applied to a posterior plane (e.g. P9D5 has more volume of bone exceeding preselected strain range than P12D5).

Strain limits of 0.2% and -0.2% were selected for maximum and minimum principal strain, although the limits are close to the reported peak of physiological strain but far less than apparent yield strain of bone [27,28,31]. Therefore, the high percentage of bone volume greater than the preselected strain range does not necessarily imply bone yield.

For a given loading condition, micromotions at a frictional contact surface are related to the contact area: a smaller area of contact results in higher micromotions. For a bone with a defect, the contact area between bone and implants decreases with increasing defect width and/depth. Therefore, the largest micromotions for each loading scenario are significantly related to both defect depth and width. Micromotions at the implant-bone interface are largely influenced by defect depth, rather than width. In the presence of posterior or medial tibial defects, asymmetric cones which reduce the lever arm and provide larger frictional areas may be useful to consider.

In the current study, to delineate the effect of the metaphyseal cone alone on the mechanical environment of the proximal tibia the evaluations were undertaken without a stem. Though stems would invariably be used by surgeons as part of the rTKA construct, and have other potential roles in terms of aiding tibial alignment, our study suggests that, from a purely biomechanical perspective, stems may not always be necessary. Peak

micromotions were found to be small even for the largest defect case managed using a tritanium cone. These small absolute micromotion values at the implant-bone interface imply that successful osteointegration would be expected in all types of defects considered in this study [19,32]. A computational study examining three designs of primary TKA cementless tibial tray using various loading scenarios, found that there was a small area of the bone-implant interface with micromotion exceeding 150 μm and that the peak micromotion was up to 225 μm [33]. The tritanium cone, therefore, appears to outperform uncemented primary tibial baseplates in terms of micromotion [33] and thus appears to be an acceptable choice for bone defect management in rTKA**.** This is supported by early clinical studies where a study of 62 rTKAs utilising cones confirmed the newly developed technology to be effective in restoring joint stability with no cases of aseptic loosening at a mean follow-up of 27-months [14]. The large friction coefficient between the porous coating of the cone and the bone reduces the micromotion at this interface, with cemented interfaces reducing micromotion even further. An experimental investigation of the same tritanium cones, in composite tibias without defects reported peak average micromotion of only 36 μm [13]. This reported value was slightly higher than the micromotions obtained from the current computational study. This could be due to the difference in material properties of bone used in the published experimental study and the current computational study: composite tibias utilised in the experimental study [13] had a lower reported Young's modulus of trabecular bone compared to the modulus used in the current study (210 MPa compared with 455 MPa used in the current study). Additionally, the stairs decent loading pattern was applied for 10,000 cycles in the above-cited study which may increase the micromotions at the bone-implant interface due to the development of plastic strain at the interface. This accumulation of permanent micromotion with increasing number of cycles at the bone-implant interface has also been observed in previous experimental [34] and computational [35] studies.

Limitations of the current study include the modelling of bone as homogeneous, isotropic and linearly elastic.The properties of proximal tibial bone are known to vary with the distance from the articular surface. This complexity was not included in our model as at rTKA bone has already been removed for primary implants with alteration of the loading environment also affecting the local bone architecture. Bone properties also change with ageing, and through disease processes including arthritis and implant loosening/osteolysis. Similarly, this aspect was not considered in the current models. This generic computational model employed homogeneous properties for trabecular and cortical bone with the aim of the trends observed being applicable to a wider range of patients. However, future studies should seek to determine if the conclusions drawn here are applicable to a wider range of patient scenarios by graduating the material properties of bone, or by examining

patient specific models. The assumptions made here to simplify modelling have been commonly used in several previous studies [15,36–38] and would not be expected to alter the trends observed for defect depth and/or width dependent strain distribution and micromotions. This has enabled many different defect geometries and locations to be investigated in a way that cannot be performed experimentally due to difficulties measuring internal bone strains and micromotions. Material nonlinearity was not included in the model and may influence the stress-strain environment at the bone-implant interface [21]. Including material nonlinearity is unlikely to alter the trends of strain distribution and micromotion. Bone is recognised as a time-dependent material [39–41]. Such time-dependent properties may accentuate loosening at the bone-implant interface when cyclic loading is applied [35], and the interfacial micromotions are also related to loading frequencies. [42]. The biomechanical performance of the cone to be used for rTKA under physiological cyclic loading needs further study by inclusion time-dependent response of bone in the computational model. Though in practice, short or long stems would typically be used in addition to symmetric cones, the cones were modelled in the absence of stems so as to better define the role of the cone itself in construct biomechanics. This study did not investigate micromotion or bone strain in an unaugmented standard tibial base plate for these defects. This was not done as it was thought unlikely that this would be used clinically, though it may have been interesting. The study did not compare cones and augments, which could potentially be used to manage suitable medial or lateral defects, but not anterior or posterior ones.

Conclusion

This generic computational model has considered a range of uncontained AORI type T2A and T2B bone defects, varying by location, width and depth and reflecting the range of defects typically encountered during rTKA surgery. The tritanium cone design performed well as a replacement for the tibial bone loss encountered in these defects in terms of both strain distribution of bone and micromotions at the bone-implant interface. Compared to the bone without defects, anterior and lateral defects do not significantly alter strain distribution. For bone with medial defects, strain distribution is most sensitive to defect width; while strain distribution for posterior defects is associated with both defect width and depth. Asymmetric cones which reduce the lever arm and provide larger frictional areas may be useful specifically in tibias with these posterior or medial defects. The micromotions at the bone-implant interface for all of the scenarios modelled are small and imply that successful osteointegration would occur in all types of defects considered in this study.

Acknowledgement

This work was supported by the EPSRC [Grant EP/K036939/1] and Stryker.

References

[1] National Joint Registry for England and Wales. 15th Annual Repor 2018. 2018.

[2] NHS Scotland. Scottish Arthroplasty Project Annual Report. Inf Serv Div NHS Scotl 2018:1–65.

[3] Derome P, Sternheim A, Backstein D, Malo M. Treatment of Large Bone Defects With Trabecular Metal Cones in Revision Total Knee Arthroplasty. J Arthroplasty 2013;29:122–6. doi:10.1016/j.arth.2013.04.033.

[4] Engh GA, Ammeen DJ. Bone loss with revision total knee arthroplasty: defect classification and alternatives for reconstruction. Instr Course Lect 1999.

[5] Scuderi GR, Parisi TJ, Dennis DA, Lewallen DG, Windsor RE, Ponzio DY. Management of Tibial Bone Loss. Complex Cases Total Knee Arthroplast., Springer; 2018, p. 245–67.

[6] Vasso M, Beaufils P, Cerciello S, Schiavone Panni A. Bone loss following knee arthroplasty: Potential treatment options. Arch Orthop Trauma Surg 2014;134:543–53. doi:10.1007/s00402-014-1941-8.

[7] Hilgen V, Citak M, Vettorazzi E, Haasper C, Day K, Amling M, et al. 10-Year Results Following Impaction Bone Grafting of Major Bone Defects in 29 Rotational and Hinged Knee Revision Arthroplasties. Acta Orthop 2013;84:387–91. doi:10.3109/17453674.2013.814012.

[8] Ghazavi MT, Stockley I, Yee G, Davis A, Gross AE. Reconstruction of massive bone defects with allograft in revision total knee arthroplasty. J Bone Jt Surg - Ser A 1997;79:17–25. doi:10.2106/00004623-199701000-00002.

[9] Patel J V., Masonis JL, Guerin J, Bourne RB, Rorabeck CH. The fate of augments to treat type-2 bone defects in revision knee arthroplasty. J Bone Joint Surg Br 2004;86-B:195–9. doi:10.1302/0301-620x.86b2.13564.

[10] Kamath AF, Lewallen DG, Hanssen AD. Porous tantalum metaphyseal cones for severe tibial bone loss in revision knee arthroplasty: A five to nine-year follow-up. J Bone Jt Surg - Am Vol 2015;97:216–23. doi:10.2106/JBJS.N.00540.

[11] Lachiewicz PF, Bolognesi MP, Henderson RA, Soileau ES, Vail TP. Can tantalum cones provide fixation in complex revision knee arthroplasty? Clin Orthop Relat Res 2012;470:199–204. doi:10.1007/s11999-011-1888-9.

[12] Meneghini RM, Lewallen DG, Hanssen AD. Use of porous tantalum metaphyseal cones for severe tibial bone loss during revision total knee replacement. J Bone Jt Surg - Ser A 2008;91:131–8. doi:10.2106/JBJS.F.01495.

[13] Faizan A, Bhowmik-Stoker M, Alipit V, Kirk AE, Krebs VE, Harwin SF, et al. Development and Verification of Novel Porous Titanium Metaphyseal Cones for Revision Total Knee Arthroplasty. J Arthroplasty 2017;32:1946–53. doi:10.1016/j.arth.2017.01.013.

[14] Denehy K, Abhari S, Krebs VE, Higuera-Rueda CA, Samuel LT, Sultan AA, et al. Excellent Metaphyseal Fixation Using Highly Porous Cones in Revision Total Knee Arthroplasty. J Arthroplasty 2019.

[15] Scott CEH, Eaton MJ, Nutton RW, Wade FA, Evans SL, Pankaj P. Metal-backed versus all-polyethylene unicompartmental knee arthroplasty. Bone Joint Res 2017;6:22–30. doi:10.1302/2046-3758.61.BJR-2016-0142.R1.

[16] Abdul-Kadir MR, Hansen U, Klabunde R, Lucas D, Amis A. Finite element modelling of primary hip stem stability: The effect of interference fit. J Biomech 2008;41:587–94. doi:10.1016/j.jbiomech.2007.10.009.

[17] Kuiper JH, Huiskes R. Friction and stem stiffness affect dynamic interface motion in total hip replacement. J Orthop Res 1996;14:36–43. doi:10.1002/jor.1100140108.

[18] Rancourt D, Shirazi-Adl A, Drouin G, Paiement G. Friction properties of the interface between porous-surfaced metals and tibial cancellous bone. J Biomed Mater Res 1990;24:1503–19.

353 doi:10.1002/jbm.820241107.

354 [19] Viceconti M, Muccini R, Bernakiewicz M, Baleani M, Cristofolini L. Large-sliding contact elements
355 accurately predict levels of bone-implant micromotion relevant to osseointegration. J Biomech
356 2000;33:1611–8. doi:10.1016/S0021-9290(00)00140-8.

357 [20] Frank RM, Fabi D, Levine BR. Modern porous coatings in orthopaedic applications. Thin Film.
358 Coatings Biol., Springer; 2013, p. 69–103.

359 [21] Donaldson FEE, Pankaj P, Simpson AH. Bone properties affect loosening of half-pin external fixators at
360 the pin – bone interface. Injury 2012;43:1764–70.

361 [22] Completo A, Simões JA, Fonseca F, Oliveira M. The influence of different tibial stem designs in load
362 sharing and stability at the cement-bone interface in revision TKA. Knee 2008;15:227–32.
363 doi:10.1016/j.knee.2008.01.008.

364 [23] Stryker. Engineered for bone. 2017.

365 [24] Bergmann G, Bender A, Graichen F, Dymke J, Rohlmann A, Trepczynski A, et al. Standardized loads
366 acting in knee implants. PLoS One 2014;9. doi:10.1371/journal.pone.0086035.

367 [25] Completo A, Fonseca F, Simões JA. Finite Element and Experimental Cortex Strains of the Intact and
368 Implanted Tibia. J Biomech Eng 2007;129:791. doi:10.1115/1.2768382.

369 [26] Nadorf J, Kinkel S, Gantz S, Jakubowitz E, Kretzer JP. Tibial revision knee arthroplasty with
370 metaphyseal sleeves: The effect of stems on implant fixation and bone flexibility. PLoS One
371 2017;12:e0177285. doi:10.1371/journal.pone.0177285.

372 [27] Pankaj P. Patient-specific modelling of bone and bone-implant systems: the challenges. Int J Numer
373 Meth Bio 2013;29:233–49.

374 [28] Levrero-Florencio F, Margetts L, Sales E, Xie S, Manda K, Pankaj P. Evaluating the macroscopic yield
375 behaviour of trabecular bone using a nonlinear homogenisation approach. J Mech Behav Biomed Mater
376 2016;61:384–96.

377 [29] Pankaj P. Computational biomechanics of bone. In: Simpson H, Peter A, editors. Exp. Res. Methods
378 Orthop. Trauma, 2015.

379 [30] MacLeod AR, Simpson AHRW, Pankaj P. Reasons why dynamic compression plates are inferior to
380 locking plates in osteoporotic bone: a finite element explanation. Comput Methods Biomech Biomed
381 Engin 2015;18:1818–25.

382 [31] Pankaj P, Donaldson FE. Algorithms for a strain-based plasticity criterion for bone. Int J Numer Meth
383 Bio 2013;29:40–61.

384 [32] Pilliar RM, Lee JM, Maniatopoulos C. Observations on the Effect of Movement on Bone Ingrowth into
385 Porous-Surfaced Implants. Clin Orthop Relat Res 1986;208:108–13. doi:10.1097/00003086-198607000-
386 00023.

387 [33] Taylor M, Barrett DS, Deffenbaugh D. Influence of loading and activity on the primary stability of
388 cementless tibial trays. J Orthop Res 2012;30:1362–8. doi:10.1002/jor.22056.

389 [34] Cristofolini L, Affatato S, Erani P, Tigani D, Viceconti M. Implant fixation in knee replacement:
390 Preliminary in vitro comparison of ceramic and metal cemented femoral components. Knee
391 2009;16:101–8. doi:10.1016/j.knee.2008.08.006.

392 [35] Xie S, Manda K, Pankaj P. Time-dependent behaviour of bone accentuates loosening in the fixation of
393 fractures using bone-screw systems. Bone Joint Res 2018;7:580–6. doi:10.1302/2046-3758.710.bjr-
394 2018-0085.r1.

395 [36] Danese I, Pankaj P, Scott CEH. The effect of malalignment on proximal tibial strain in fixed-bearing
396 unicompartmental knee arthroplasty. Bone Jt Res 2019;8:55–64. doi:10.1302/2046-3758.82.BJR-2018-
397 0186.R2.

398 [37] Conlisk N, Howie CR, Pankaj P. Quantification of interfacial motions following primary and revision
399 total knee arthroplasty: A verification study versus experimental data. J Orthop Res 2017:1–10.

doi:10.1002/jor.23653.

[38] Conlisk N, Howie CR, Pankaj P. Optimum stem length for mitigation of periprosthetic fracture risk following primary total knee arthroplasty: a finite element study. Knee Surgery, Sport Traumatol Arthrosc 2018;26:1420–8. doi:10.1007/s00167-016-4367-8.

[39] Xie S, Manda K, Wallace RJ, Levrero-Florencio F, Simpson AHRW, Pankaj P. Time Dependent Behaviour of Trabecular Bone at Multiple Load Levels. Ann Biomed Eng 2017;45:1219–26.

[40] Manda K, Xie S, Wallace RJ, Levrero-Florencio F, Pankaj P. Linear viscoelasticity - bone volume fraction relationships of bovine trabecular bone. Biomech Model Mechanobiol 2016;15:1631–40.

[41] Manda K, Wallace RJ, Xie S, Levrero-Florencio F, Pankaj P. Nonlinear viscoelastic characterization of bovine trabecular bone. Biomech Model Mechanobiol 2016;16:173–89.

[42] Xie S, Manda K, Pankaj P. Effect of loading frequency on deformations at the bone–implant interface. Proc Inst Mech Eng Part H J Eng Med 2019:095441191987797. doi:10.1177/0954411919877970.

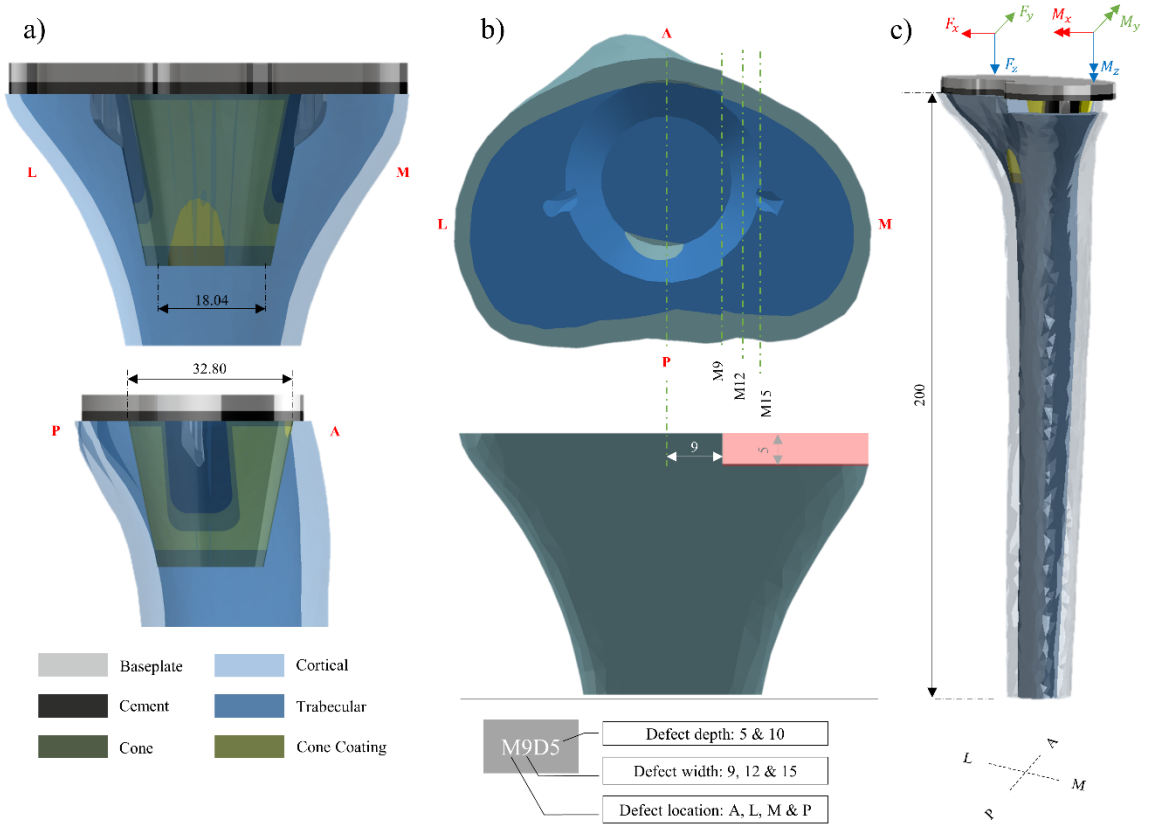

Figure 1 The implant system consists of 4 parts with different materials assigned: baseplate, cement (2mm in depth to avoid direct metal contact between baseplate and cone), titanium cone and titanium cone coating (a); illustration of a bone defect (or bone loss) encountered in revision total knee arthroplasty at varying widths and depths considered (only one of the four locations considered is shown) (b); tibial bone was considered in the analysis, and the positive axes point to lateral, anterior and inferior directions for F_x, F_y and F_z respectively, and for positive moments (c)

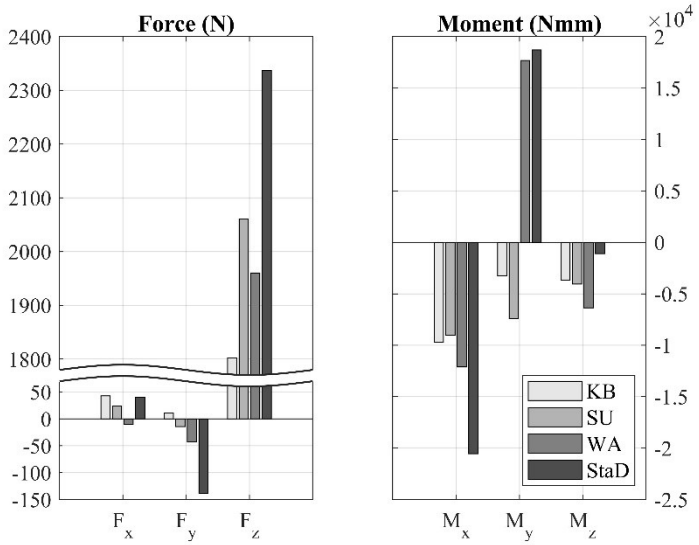

422

423 Figure 2 Loadings applied. Six degrees of freedom were considered for load application, three forces and three
424 moments. Four loading scenarios were considered: knee bend or squatting (KB) standing up (SU), walking
425 (WA) and descending stairs (StaD)

426

427

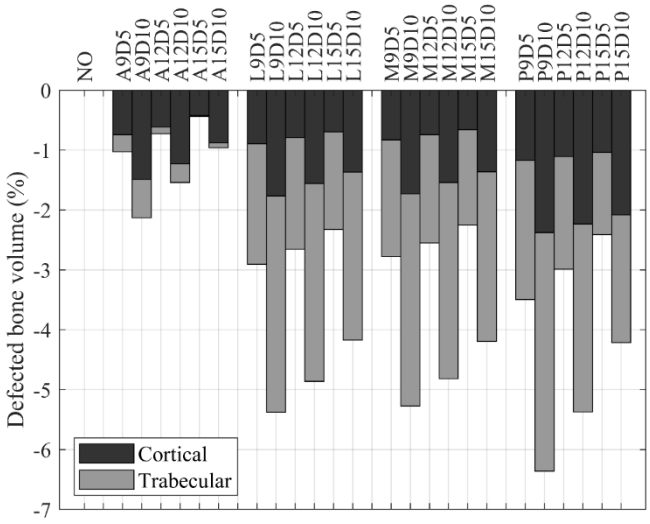

428

429 Figure 3 Bone loss as a percentage of total bone volume for all 24 defects considered in this study

430

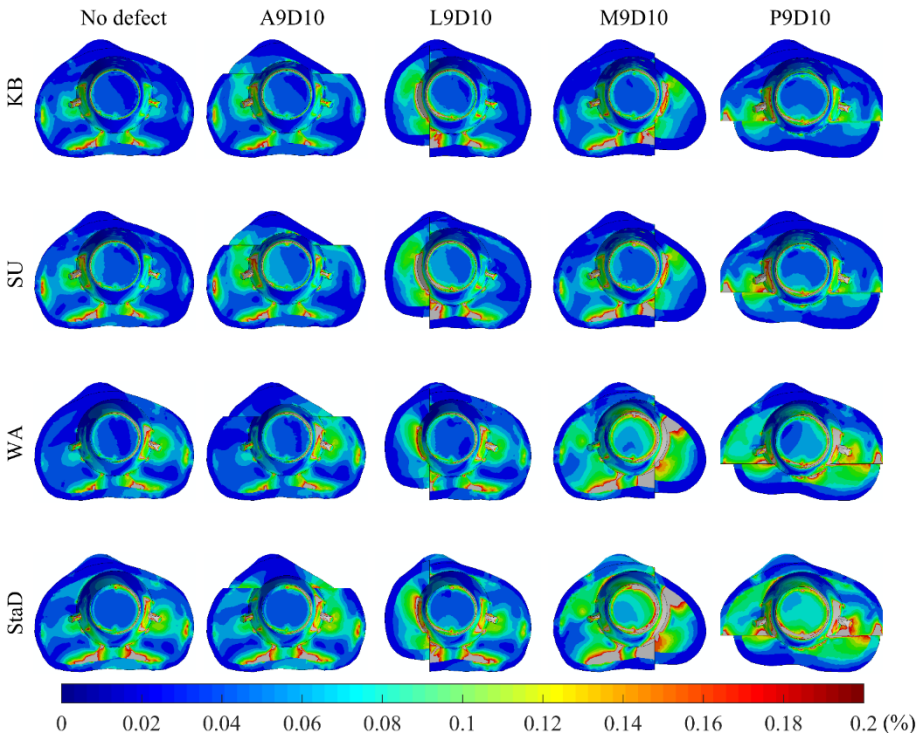

(a)

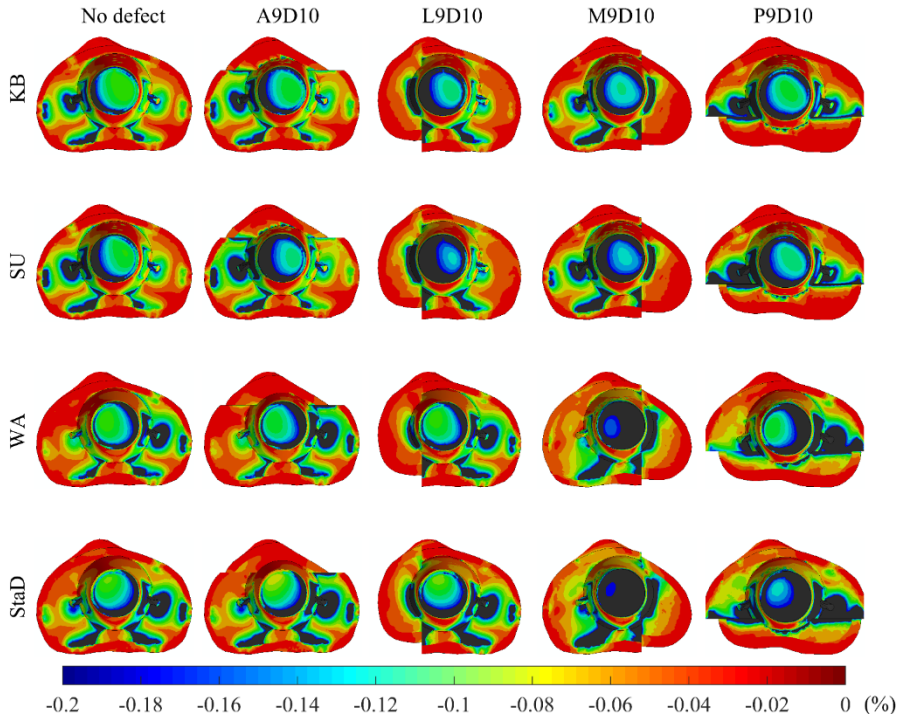

(b)

Figure 4 Maximum (a) and minimum (b) principal strain (%) contours superior view for all loading scenarios for selected bone defects. Only bone without defect and severest bone defect for each anatomic location are shown in this contour plot

438

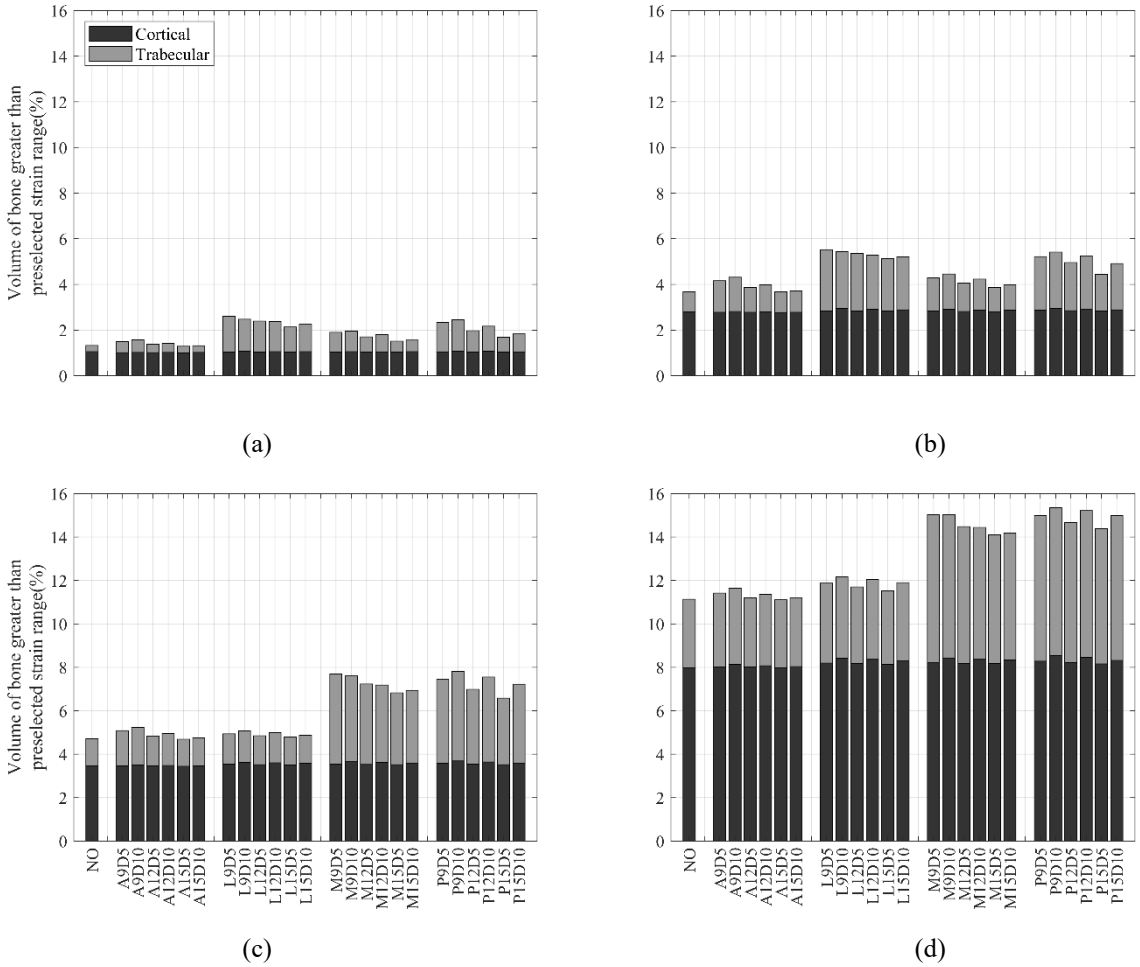

Figure 5 Comparison of the volume of bone that exceeds the preselected principal strain magnitude of 0.2% (0.2% and -0.2% for maximum and minimum principal strain, respectively) for: knee bend (a); standing up (b); walking (c); descending stairs (d)

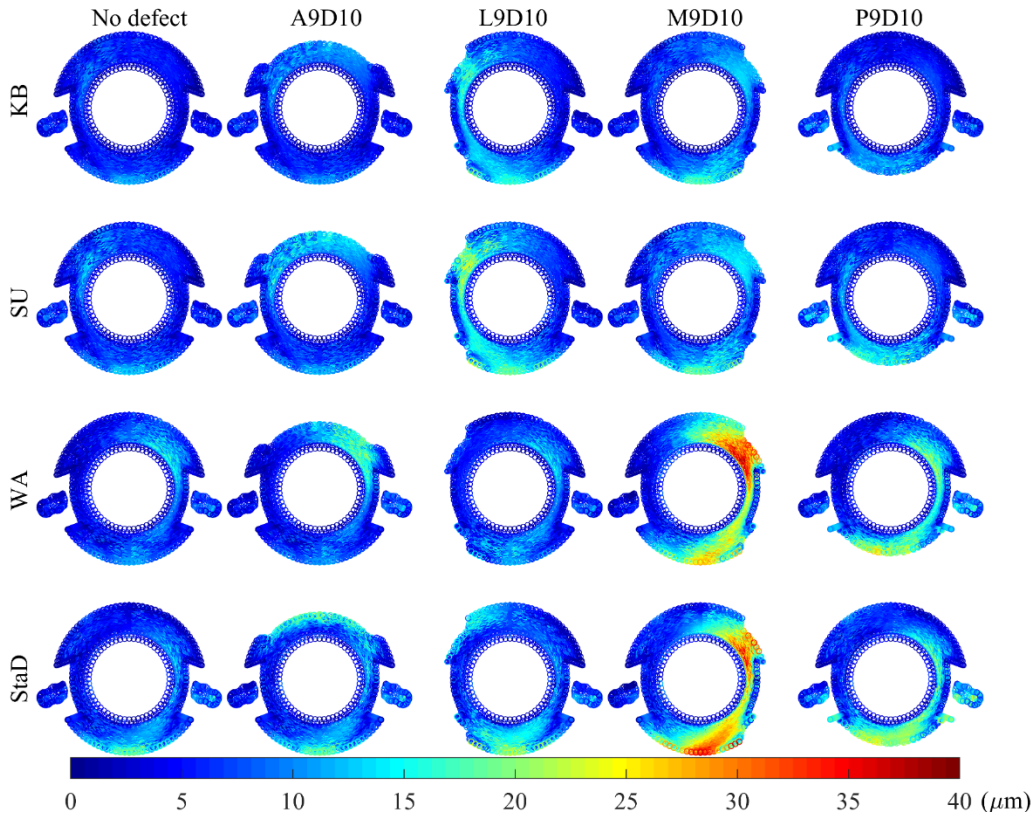

Figure 6 Superior view of micromotion contours at bone-implant interface for all loading scenarios for selected bone defects. Only bone without defect and severest bone defect for each anatomic location are shown in this contour plot

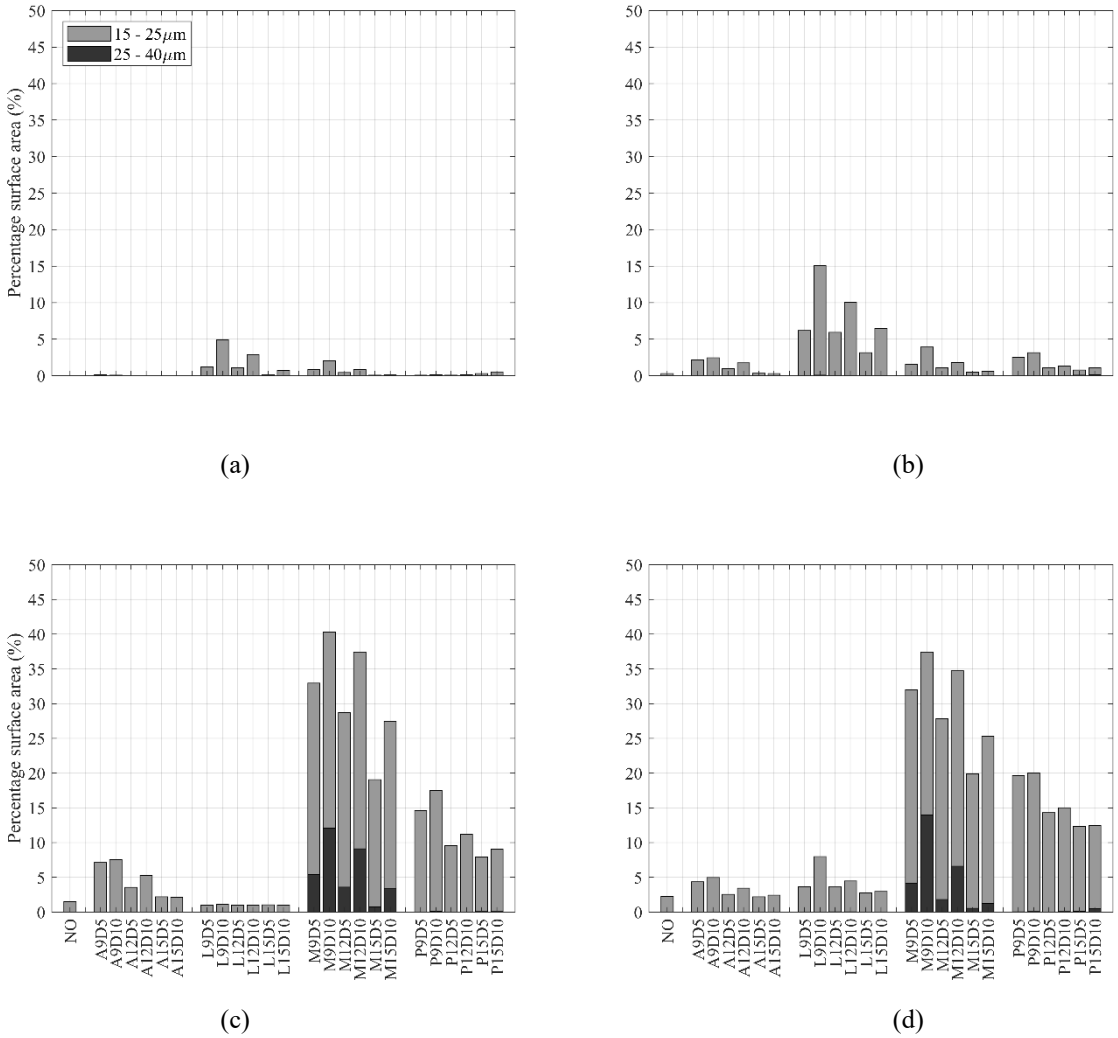

(a) (b)

(c) (d)

Figure 7 Comparison of the predicted micromotions occurring at the bone-implant interface by range for: knee bend (a); standing up (b); walking (c); descending stairs (d);